Quantum Mechanical Modeling of the Complexation of Actinides by Humic Substances

Abschlussbericht für das Teilprojekt „Quantenmechanische Modellierung der Komplexierung von Actinoiden durch Huminstoffe“

im Rahmen des Verbundprojektes „Migration von Actinoiden im System Ton, Huminstoff, Aquifer“

Förderkennzeichen 02E9693

Projektlaufzeit Juli 2003 bis Juni 2006

Notker Rösch und Sven Krüger
Department Chemie, Theoretische Chemie
Technische Universität München
85747 Garching

Das diesem Bericht zugrundeliegende Vorhaben wurde mit Mitteln des Bundesministeriums für Wirtschaft und Arbeit unter dem Förderkennzeichen 02E9693 gefördert. Die Verantwortung für den Inhalt der Veröffentlichung liegt bei den Autoren.

1 Introduction

The versatile complexation chemistry of actinide elements strongly affects their distribution and their transport in the environment [1-3]; other important factors are colloid formation and the large variety of solid phases [4,5]. The behavior of actinides under natural conditions is determined not only by their solubility and complexation in aqueous solution, but also by the interaction of aqueous species with soils, minerals, and natural organic matter [6,7]. Sorption and colloid formation strongly influence the chemical state as well as the transport behavior of actinide ions. In turn, migration of actinides is a central issue in safety analysis and long-term storage modeling for predicting the distribution and the behavior of actinides in the environment, especially with regard to radioactive waste management as well as remediation of contaminated sites of uranium mining and former nuclear weapon production. Whereas the aquatic chemistry of the more common oxidation states of actinides is now fairly well understood [1,3,8], much less is known regarding sorption at mineral surfaces and interaction with natural organic matter. These two topics form the subject of the research organized by the consortium "Migration von Actinoiden im System Ton, Huminstoff, Aquifer". Modeling of the interaction of humic materials with actinides by quantum chemistry methods was the central topic of one of the involved projects, the results of which will be discussed in the following.

Humic substances form an important class of natural organic matter [9], which is ubiquitous in the lower geosphere, besides other organic molecules, like carboxylic acids. They originate from the metabolism of organisms or the degradation of biological materials. Humic substances are an essential component of soils, but they also are present in surface and ground waters [9]. They complexate metal ions and are redox active and thus noticeably affect the speciation and the distribution of metals in the environment [6,7,9]. Their more solubale fraction, humic and fulvic acids [9], is formed by very variable larger organic molecules, that exhibit a variety of functional groups. Among them, carboxyl groups are considered to be most important for metal and, specifically, actinide complexation [10-15]. Only recently several studies began to inspect possible contributions of other functional groups to actinide complexation of humic substances [16-18]. Thus far, the structure of actinide carboxylate and humate complexes is accessible mainly indirectly from EXAFS experiments [19] via analogy with definite data from crystal structures. Also the interpretation of the results of other spectroscopic approaches to actinide complexes of humic acids rely on analogies [18,20,21]. There are quite a number of experimental studies on the interaction of actinides with humic acids [12,13,15,19-23] and also on the effect of humic substances on actinide sorption and colloid formation [11,24,25]. However, a comprehensive understanding of these processes on the atomic scale is still lacking, also due to experimental difficulties that result from the heterogeneity of humic substances.

The main goal of the present project was to complement current knowledge on actinide interaction with humic substances, which largely originates from experiments, by means of quantum chemical calculations. Modeling of actinide complexation by relevant organic functional groups provides new insights at the atomic level. Modern quantum chemistry methods, e.g. those derived from relativistic density functional theory, were applied to provide accurate geometric, spectroscopic as well as energy data [26-28], which are directly related to relevant and well-defined species. Thus, these data are useful for interpreting spectroscopic results, especially when geometric models are involved as in the interpretation of EXAFS measurement. The results of this project also provide insight into bonding mechanisms, solvation effects, and other detailed chemical and physical features that will foster an understanding of similarities and differences of actinide complexes.

2 Tasks of the Project and Prerequisites

The project was mainly concerned with modeling the complexation of actinyl ions by humic substances with the help of quantum chemical methods. The basic modeling strategy relied on replacing functional groups of humic substances by analogous small organic molecules that represent a single and isolated active site. The same approach to studying simple species as model compounds and to understanding actinide complexation at the atomic level has earlier been put forward in experimental studies [29-31]. An accurate relativistic density functional method [32,33] was employed to calculate electronic and geometric structures of actinide complexes in solution as well as their energetic parameters. For this purpose, the high-performance software PARAGAUSS [34] was employed. In addition, a polarizable continuum model [35] was used to account for long-range (electrostatic) solvation effects. The latter method had been implemented in the software package PARAGAUSS during the preceding project 02E9450. Short-range chemical interactions with the solvent were modeled by means of aqua ligands, explicitly included in the quantum chemical models [35].

The central topic of the project was the characterization of complexes of actinyls, mainly of uranyl(VI), with organic ligands. In this way the variability of properties of functional groups was characterized by varying model ligands that mimic different chemical surroundings present in larger molecules like humic acids. The results were then compared to experimental data, assisting their interpretation at the atomic level. The overall picture emerging may also be compared to empirical speciation and complexation models for actinide interaction with humic substances [36,37]. Here, energetic parameters as well as the qualitative compareson of different functional groups are of particular interest. Besides these goals, also other issues, e.g., the determination of fundamental thermochemical parameters of uranyl or the sorption of uranyl on mineral surfaces were addressed, as inspired by the work of partner projects in this cooperative initiative.

The project was divided into the following tasks:

- **Complexes of simple aliphatic carboxylates**
  The most simple aliphatic carboxylic acids were treated as model ligands to study various complexation modes, geometries, and energetics as well as the variation of these properties with increasing aliphatic chain length. This class of ligands served as central reference and as benchmarks to verify methods and modeling strategies.

- **Complexes of derivatives of carboxylates and aromatic carboxylates**
  A broad investigation of various carboxylic ligands was carried out to explore the variability of properties of possible carboxylic sites in humic substances. By comparison to experimental findings these results were intended to yield information about the atomistic structure and the thermochemical properties of actinide humate complexes.

- **Complexes with alternative functional groups**
  Focusing on alcoholic groups, alternative functional groups of humic acids were investigated and compared to carboxylic groups. Previously, carboxylic functionalities were taken almost exclusively into account in experimental studies. This task supported experimental activities of the project partner Institute of Radiochemistry at the Forschungszentrum Dresden-Rossendorf which inspected the role of phenolic OH groups in actinide complexation.

- **Models of humic acids**
  While starting with small organic molecules as models (see above), it was necessary to explore their adequacy as models and the potential need to account for a wider chemical environment when aiming at the proper representation of active centers of humic substances. Results of earlier tasks would then have to be compared to larger carboxylic acids and to enhanced models which relied on a combined quantum mechanical and molecular mechanical approach (QM/MM), where the distant environment of a complexation site would approximately be described by a classical force field.

- **Method development**
  For the treatment of actinide complexes in solution appropriate parameters for the polarizable continuum model had to be determined and verified. Implementation of a QM/MM method for larger models of humic acids was intended if results of previous tasks indicated the need. In addition, a discrete solvation model of QM/MM type had to be implemented which allows an efficient treatment of a larger number of solvent molecules around the model complexes. For this purpose, a commonly applied force field for water was combined with the polarizable continuum treatment for long-range solvation effects. In this way an accurate representation of the discrete nature of the solvent environment was achieved. In addition, the relativisitic density functional

methods applied had to be supported and extended as required by the other tasks of the project.

A prerequisite for the large number of demanding electronic structure calculations and geometry optimizations performed in this project was the application of an efficient high-performance software for computers with parallel architecture. These requirements are satisfied by the density functional package ParaGauss [34], which is available on various hardware platforms. The Linux cluster of the group executing the project, currently comprising about 100 CPUs, was essential for the success of the project. In the framework of this project, four dedicated two-processor nodes had been granted, which had been put into operation for the second half of the project.

3 Development of the State of the Art

Computational modeling of actinide complexes in solution as the central topic of the project represents a challenge for quantum chemistry because several complications have to be faced simultaneously. Actinides are very heavy elements; therefore, a relativistic treatment is indispensable. Actinide ions exhibit several open valence shells which requires a careful treatment of electron correlation. For very accurate calculations on open-shell complexes also spin-orbit interaction may have to be considered. In addition to these aspects related to the electronic structure, solvent effects have to be taken into account. In the following, we will briefly discuss the state of the art and recent developments of pertinent computational techniques and their application to actinide complexes, focusing on solution chemistry. For more detailed presentations of the field, the reader is referred to recent reviews [26-28].

The most popular strategy to account for relativistic effects in heavy atoms relies on effective core potentials (ECPs, "pseudopotentials") [38,39]. Thereby, one represents the effect of core electrons of a heavy atom by a relativistically determined pseudopotential; this allow a conventional nonrelativistic treatment of the valence electronic structure. Explicitly relativistic methods, with which one is able to describe larger actinide complexes, invoke a quasi- (or scalar) relativistic approximation to the Dirac-Kohn-Sham method that may include spin polarization. Of practical importance in actinide chemistry are the ZORA approach [40,41] and the Douglas-Kroll-Hess method [32,33]. The latter was used in this project. Fully relativistic four-component methods or self-consistent two-component approaches including spin-orbit interaction are still restricted to small molecules, without any environmental modeling. For the example of PuN_2 it was recently demonstrated by means of an accurate CASPT2 calculation and a subsequent treatment of spin-orbit interaction that spin-orbit effects are small for actinide compounds with only few electrons in the open f shell ($5f^2$) [42]; this is a consequence of the localization of the f-electrons on the actinide center. Also for electron transfer reactions in mixed valent complexes of Np(VI) and Np(V) it was shown that spin-orbit effects hardly affect activation energies [43].

Long-range solvation effects on molecules are commonly modeled by means of polarizable continuum models (PCM) where the molecule is placed in a cavity inside a dielectric continuum that is constructed mainly as superposition of atom-centered spheres [44]. This modeling approach may be complemented by empirical corrections for some short-range interactions (e.g. cavity formation). However, this modeling approach does not account for short-range chemical interactions of solvent molecules; rather, they have to be accounted for by including water molecules in the model treated quantum mechanically. This has been shown to be necessary for an accurate description of charged solutes like actinyls; in recent years, this combination approach of an explicitly treated first solvation shell supplemented by a PCM has been established as standard for describing actinide complexes in solution [27,45]. We had developed and applied this modeling strategy even earlier [35,46,47] and used it throughout this project.

Recent studies showed that the successful application of the PCM approach rests on a careful design of the physical model and a judicious choice of the cavity type and pertinent parameters [48,49]. The limitations of the explicit first shell model recently were explored for the solvated uranyl ion as test system where, in some models, also the second solvation shell was represented in a restricted fashion. Changes of bond lengths of uranyl up to 0.01 Å and stronger effects on the bonds with the aqua ligands were observed as well as a nonnegligible charge transfer from the second shell [48,50]. Explicit inclusion of the second shell only marginally affected the solvation energy; also, the second solvation shell alone accounted for all essential effects when an aqua ligand is removed from the first ligand shell [48]. To avoid the rather demanding quantum mechanical treatment of a larger solvation environment, a QM/MM approach has been invoked [51,52]. In this way the discrete nature of the solvent can be represented more realistically. For $[UO_2(OH)_4(H_2O)_n]^{2-}$ it was shown that an accurate description of structures and charge distribution is possible by restricting the quantum mechanical system to the first solvation shell, but energies were corrected by single-point quantum chemistry calculations using a larger cluster model [51]. For $[UO_2F_4(H_2O)_n]^{2-}$ it was shown that only by means of an explicit quantum mechanical model of the first solvation shell of 11 aqua molecules the experimentally determined fivefold coordination of uranyl could be reproduced [52]. Recently, Car-Parinello “first principles” molecular dynamics (CPMD) was applied for the first time to solvated actinide complexes [53]. The exchange of an aqua ligand [54] as well as the acidity of solvated uranyl [55] were explored, reproducing experimental values within about 10 kJ/mol. For mixed uranyl nitrate hydroxide and nitrate tetramethylmalonamide complexes solvation effects of the much more demanding CPMD method and the ZORA/PCM approach were shown to agree well [56].

From these examples one may conclude that a solvation treatment exceeding the explicit inclusion of a first solvation shell, combined with a PCM treatment, will be only necessary when properties are examined that crucially depend on the discrete nature of the

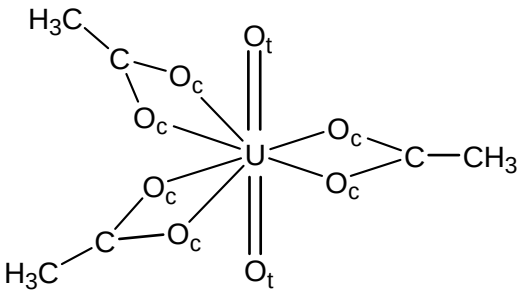

Figure 1. Sketch of the structure of uranyl(VI) triacetate.

molecule-solvent interaction. In view of this result, we elaborated a combined QM/MM-PCM procedure in ParaGauss (Section 4.6).

In recent years, only few computational studies were devoted to uranyl carboxylate complexes, the main topic of this project. Ion trap experiments for the hydration of uranyl monoacetate in the gas phase showed that up to three aqua ligands are attached to this complex, leading to a four- or five-fold coordination of uranyl by equatorial ligands which may vary with the coordination mode of the ligands [57]. Accompanying density functional calculations on $UO_2(CH_3COO)(H_2O)_3$ determined the energy difference between these two coordination modes to be by only 2 kJ/mol [57]. Uranyl acetate complexes with one to three ligands were studied with ECP density functional calculations [58], but this study did not include explicit aqua ligands or long-range solvation effects. As a result, much stronger variations of uranyl vibrational frequencies than inferred from crystalline probes were calculated. Although oxalate can not be regarded as a model for complexation by humic acids, it is of interest as ligand exchange mechanisms as well as the chelate effect have been studied in detail for this carboxylic acid [3]. To the best of our knowledge, the interaction of uranyl with alcoholic groups has not been treated computationally until now. Thus, the results provided in this project fill a gap, especially with respect to data which may be helpful for interpreting experimental studies on actinyl humate complexation and the construction of empirical complexation models.

4 Results

Here, we will review the main results of the project following the project plan. First we will present computational results for actinyl complexation by organic ligands and their impact on the current view on actinyl humate complexes. Then we will describe studies on the thermochemistry of actinyls. Finally we will review methodological work on relativistic density functional methods and solvation models. Where publications are already available, the presentation will be more concise. Project-related publications are listed in Section 6 and also included among the references.

Table 1. Geometric parameters (in Å) und symmetric stretching frequency of uranyl (ν_s, in cm^{-1}) of uranyl(VI) triacetate $[UO_2(OOCCH_3)_3]^-\cdot(H_2O)_n$ for bidentate ligand coordination. Results obtained with LDA (VWN) and GGA (BP, PW91) exchange-correlation potentials are compared with experimental results form aqueous solution (Sol.) and crystal structures (Cryst.). Gas phase (GP) and solvated (PCM) model results without and with n additional explicit aqua ligands are compared. For the designations of atoms, see Figure 1.

	n	XC	U=O_t	U-O_c	U-C	U-CH_3	ν_s
Exp.							
Sol.[a]			1.78(2)	2.44(2)	–	4.34	823
Cryst.[b]			1.78(1)	2.48(2)	2.88(3)	–	–
LDA							
GP	0	VWN	1.792	2.449	2.816	4.315	837
GP	3	VWN	1.783	2.459	2.848	4.337	857
PCM	0	VWN	1.803	2.424	2.817	4.299	811
PCM	3	VWN	1.792	2.438	2.849	4.323	831
GGA							
GP [c]	0	PW91	1.81	2.51	–	4.38	–
GP	0	BP	1.81	2.52	2.89	4.41	810
GP	3	BP	1.80	2.53	2.92	4.43	825
PCM[c]	0	PW91	1.81	2.50	–	4.38	–
PCM	0	BP	1.82	2.49	2.89	4.39	785
PCM	3	BP	1.81	2.50	2.91	4.41	799

[a] Refs.67,70. [b] Average, Refs. [15, 30,61,62,71]. [c] Ref. [63].

4.1 Complexes with aliphatic carboxyl ligands

Uranyl triacetate

Uranyl(VI) triacetate (Figure 1) represents a well characterized reference system for the validation of methods and models. In solution the three acetate ligands coordinate in bidentate fashion in the equatorial plane of uranyl, excluding aqua ligands from the first ligand shell. To inspect solvation effects and validate different models of solvation, gas phase as well as PCM [35] calculations have been performed, with and without explicitly modeled water ligands of the second solvation shell [59,60]. We modeled the effect of explicit aqua ligands of the second coordination shell in a qualitative way as we assumed them to bridge oxygen atoms of different carboxyl groups. The structure from a scalar relativistic density functional approach [33] in the form of a local density approximation (LDA) for the exchange correlation (XC) potential agrees very well with available experimental results in solution [67,70]. The best agreement is achieved for the model with

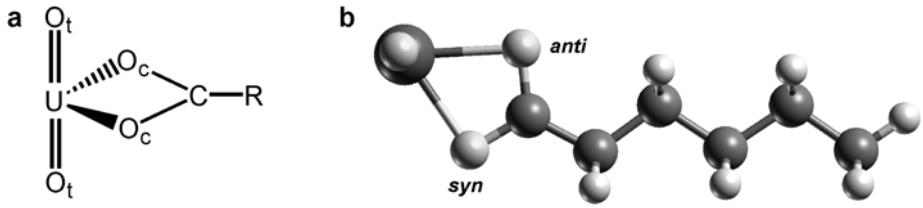

Figure 2. (a) Sketch of bidentate aliphatic uranyl monocarboxylates $[UO_2(OOCR)]^+$, R = C_nH_{2n+1}, (b) Optimized structure for n = 5 in C_s symmetry. The oxygen atoms of the carboxyl group are distinguished as *syn* ($O_{c,s}$) and *anti* ($O_{c,a}$) with respect to the C_α-H moiety of the hydrocarbon chain.

PCM embedding and additional aqua ligands. Available distances in solution agree within 0.02 Å and the symmetric uranyl stretching frequency is reproduced within 10 cm^{-1}. This has to be regarded as a good agreement for accurate density functional calculations. As LDA XC functionals are known to overestimate binding energies, single-point calculations at the level of a gradient-corrected functional (generalized gradient approximation – GGA) were carried out to obtain better estimates of energetics. As shown here for the example of uranyl triacetate, structures from GGA calculations tend to overestimate interatomic distances (Table 1, BP and PW91 functionals) [59,60].

Monocarboxylates $[UO_2OOCR]^+$ in the gas phase

The effect of ligand size and type has been examined for bidentate complexes in the gas phase with a single aliphatic carboxylate (Figure 2). The omission of solvent effects in this approximate model study should increase the sensitivity of the model since the damping effect of a polarization field and the concurrence to aqua ligands is missing. To study the influence of ligand size, the aliphatic chain length was increased. C_α substitution of acetic acid models was used as a model for the varying chemical environment of a carboxylic group in a humic acid molecule. In this way uranyl monocarboxylate complexes were constructed which are useful models for inspecting variations in the chemical properties of carboxylic groups of humic substances [60].

Tabel 2. Geometric parameters (distances in Å, angles in degree), Mulliken charges q of uranyl (in e) and symmetric stretching frequency of uranyl ν_s (in cm^{-1}) of bidentate uranyl monocarboxylates $[UO_2(OOCR)]^+$, R = C_nH_{2n+1}, for n = 0–5 in the gas phase.

n	U=O_t	O_t=U=O_t	U-$O_{c,s}$	U-$O_{c,a}$	U-C	q(UO_2)	ν_s
0	1.745	172.6	2.242	2.242	2.628	0.96	946
1	1.749	172.0	2.224	2.224	2.640	0.91	936
2	1.750	171.8	2.213	2.227	2.635	0.90	933
3	1.751	171.8	2.205	2.234	2.635	0.89	932
4	1.751	171.8	2.206	2.234	2.635	0.88	930
5	1.752	171.8	2.206	2.236	2.634	0.87	927

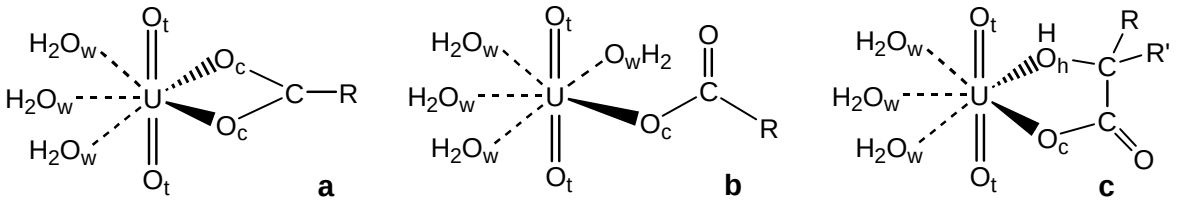

Figure 3. Schematic structure of different coordination modes of uranyl monocarboxylate complexes $[UO_2(OOCR)(H_2O)_n]^+$: a) bidentate, b) monodentate, c) chelate.

The effect of the length of the aliphatic chain on uranyl monocarboxylate complexes was studied in the gas phase for bidentate complexes, applying C_s symmetry constraints. The results for the complexes $[UO_2(OOCC_nH_{2n+1})]^+$ (n = 0–5) are collected in Table 2. With the exception of the formiate complex, a rather uniform picture arises, as expected. Interatomic distances, charge, and symmetric stretching frequency of uranyl for longer aliphatic carboxyls are very similar to the results for the acetate species. Only the difference of 0.03 Å between the two uranyl carboxylate U-O_c bonds converges later, namely for propionic acid. With increasing chain length, one notes very weak trends of decreasing uranyl charge, increasing uranyl bond length, and decreasing uranyl stretching frequency from the data of Table 2. The inspected properties converge very well for propionic acid (n = 3). This can be taken as a hint that effects of the chemical environment also in humic substances should be mainly restricted to the range of about three carbon-carbon bonds.

We modeled bidentate monocarboxylate complexes of acrylate, glycolate, and glycin in the same way and found only small differences to the acetate complex, the largest ones for glycin. Compared to other carboxylate ligands, the uranyl bond length is elongated by 0.005 Å in line with a reduced symmetric uranyl stretching frequency of the glycin complex, by 16 cm^{-1}. The corresponding U-C distance is 0.02 Å longer. Thus, also variations due to substitution close to the carboxylate group are small. Hence, one expects rather small variations of properties of aliphatically connected carboxyl functional groups in humic substances.

Monocarboxylates $[UO_2OOCR(H_2O)_n]^+$ in aqueous solution

We examined monocarboxylates of uranyl(VI) in solution as models of uranyl complexes with humic substances. However, monocarboxylates are also of interest by themselves, as they occur as a first stage of uranyl complexation by carboxylic acids or at low carboxylate concentrations. Monodentate, bidentate, and chelate complexation modes have been discussed (Figure 3). Chelate complexes require an appropriate second group besides carboxyl. Coordination n = 5 in the equatorial plane of the uranyl moiety was chosen as it is most common [29,64]. Thus, to complete the first ligand shell of uranyl, the models of monocarboxylate complexes are complemented by four aqua ligands for monodentate carboxylate

Tabelle 3. Geometric parameters (in Å) and symmetric uranyl stretching frequency ν_s (in cm^{-1}) for uranyl(VI) monocarboxylates $[UO_2(OOCR)(H_2O)_n]^+$ in bidentate (bi, n = 3), monodentate (mono, n = 4), and chelate coordination (chel, n = 3) of the carboxylate ligand in comparison to experimental data for acetate as well as averaged data for various carboxylates in solution (Sol.) and from crystal structures (Cryst.). The model results were obtained with C_s symmetry constraints and a PCM treatment of long-range solvation effects. For the designations of atoms, see Figure 3.

	R	U=O_t	U-O_c	U-O_h	U-C	U-O_w	U-O_{eq}	ν_s
bi	H	1.783	2.394		2.770	2.356	2.371	860
	CH_3	1.787	2.371		2.769	2.360	2.364	858
	CH_2CH_3	1.786	2.369		2.768	2.369	2.369	853
	CH_2OH	1.783	2.393		2.771	2.353	2.369	862
Exp.	CH_3 Solv.[a]	1.78(1)	2.50(2)		2.91(2)	2.38(2)	2.43(2)	861
	Sol.[b]	1.78(1)	2.46(4)		2.87(4)	2.40(4)	2.42(4)	–
	Cryst.[c]	1.76(3)	2.48(5)		2.86(5)	2.36(4)	2.42(6)	–
mono	H	1.788	2.221		3.400	2.415	2.376	850
	CH_3	1.790	2.201		3.401	2.421	2.377	846
	CH_2CH_3	1.790	2.201		3.401	2.421	2.377	849
	CH_2OH	1.786	2.247		3.400	2.408	2.375	852
Exp.	Sol.[b]	1.78(1)	–		–	–	2.38(4)	–
	Cryst.[c]	1.76(3)	2.39(5)		3.5(1)	2.42(6)	2.36(2)	–
chel	CH_2OH	1.790	2.229	2.423	3.272	2.380	2.359	846
Exp.	Sol.[d]	1.79(1)	–	–	3.25(3)	–	2.37(1)	–
	Cryst.[e]	1.75(1)	2.37	2.50	3.3	–	2.36(2)	–

[a] Refs. 30,69, 70, [b] Average over data from Refs. 29,30, 31, [c] Average over data from Refs. 10, 30, 71 [d] Average over data from Ref. 29 [e] Ref. 72.

coordination and by three in case of bidentate and chelate complexes. As a first approximation, we studied C_s symmetric models. The equatorial plane of the uranyl was chosen as mirror plane, leading to more stable structures than a perpendicular mirror plane [59,60]. We also applied a PCM treatment to model long-range solvation effects.

The calculated results [59,60,65] for geometries and symmetric uranyl stretching frequencies, obtained with a LDA (VWN) XC functional, for formiate, acetate, propionate, and glycolate are collected in Table 3 and compared to available experimental data. As definite experimental data for monocarboxylates are not available, we compared the calculated results to experimental findings in solution [29–31,69,70], which normally contain a mixture of species with different numbers of ligands. Also given in Table 3 are averaged

data for various carboxylates in solution [29-31] as well as geometric parameters from crystal structures [10,30,71,72], which are also used to interpret the experimental findings in solutions [29,66]. Referring to crystal structures, EXAFS results for complexes in solution have been interpreted as bidentate when the average distance between uranium and the oxygen atoms of the equatorial ligand shell, U-O_{eq}, amounts to about 2.42 Å [29-31]. For monodentate and chelate coordinated complexes, a value of about 2.36 Å has been inferred from crystal structures. As a second criterion for assigning structures, measured U-C distances can be employed: they are about 3.40 Å for monodentate complexes, notably shorter for chelate coordination (3.25), but only 2.80–2.90 Å for bidentate complexes (Table 3).

For all four ligands inspected, we compared monodentate and bidentate coordination, for glycolate also chelate coordination (Table 3). The calculated uranyl bonds of 1.78 to 1.79 Å were found to agree well with experimental results in solution; its weak variation points to similar bond strength in the complexes, independent of the coordination mode. Consequently, also the uranyl stretching frequency varies only slightly. A weak trend to softer vibrations (by ~10 cm^{-1}) was obtained for monodentate compared to bidentate complexes, but this is too small a variation to be indicative for the coordination mode of the carboxyl ligands. The bond length U-O_c depends on the coordination mode. We calculated 2.20–2.25 Å for monodentate and chelate complexes, while we obtained almost 2.40 Å for the bidentate coordination mode. This trend agrees with experiment, but the calculated bond lengths are 0.1–0.2 Å shorter than experimental values. Calculated U-C distances deviate similarly from experiment: they are ~0.1 Å too short for mono- and bidentate complexes. Yet, the value of 3.27 Å for the chelate structure agrees with the experimental result of 3.25 Å [29]. As in experimental, shorter U-C distances (2.77 Å) were calculated for bidentate and longer ones (3.40 Å) for monodentate complexes. Thus, the *differences* of the calculated carboxyl bonds between the two coordination modes agree qualitatively with the experimental differrences. The bond lengths of aqua ligands to uranyl, U-O_w, were calculated in agreement with EXAFS results (Table 3). However, with EXAFS, it is difficult to resolve differences in interatomic distances of less then 0.1 Å; therefore, most often, one determines only the average U-O distance to equatorial ligands, U-O_{eq}. For this quantity, our calculation yielded values of 2.37±0.01 Å, irrespective of the coordination mode. This is at variance with experiment, where comparable distances, ~2.38 Å, have been assigned for monodentate and chelate complexes, but a longer value, ~2.42 Å, for bidentate coordination (Table 3). Thus, while qualitatively the characteristic differences of carboxylate bonding for various complexation modes were reproduced, the variation of U-O_{eq} was not found in the computational results [59,60].

To study further these remarkable deviations between quantum chemistry calculations and EXAFS results, we examined the effect of various model assumptions, i.e. of the assumed mirror symmetry of the structures and the five-fold coordination of uranyl. We also

Table 4. Geometric parameters (in Å) of uranyl(VI) monocarboxylates $[UO_2(OOCR)\cdot(H_2O)_4]^+$ with monodentate ligand coordination. Comparison of calculated results without symmetry constraints in solution (PCM) and experimental data (Exp.) from solution (Sol.) and cyrstal structures (Cryst.). ΔC_s is the averaged difference to model calculations employing C_s symmetry (Table 3). For the designations of the atoms, see Figure 3.

	R	U=O_t	U-O_c	U-C	U-O_w	U-O_{eq}	ΔE
	H	1.786	2.290	3.341	2.394	2.373	-31
	CH_3	1.789	2.291	3.352	2.382	2.364	-28
	CH_2CH_3	1.790	2.287	3.333	2.383	2.364	-30
	ΔC_s	<0.01	0.08	-0.06	-0.03	-0.01	-30
Exp.	Sol.[a]	1.78(1)	–	–	–	2.38(4)	
	Cryst.[b]	1.76(3)	2.39(5)	3.5(1)	2.42(6)	2.36(2)	

[a] Average of data from Refs. 29-31. [b] Average of data from Refs. 10, 30, and 71.

.

explored hydrolysis as a further possible rationalization for the deviation from experiment. Finally, we scrutinized the comparability of experimental and theoretical systems.

Release of the symmetry constraints of the model complexes only insignificantly changes the geometries of bidentate complexes (Table 4, Figure 4a). All relevant distances relax less than 0.01 Å [60]. For monodentate complexes, an aqua ligand rotates around the coordination direction and forms a hydrogen bond with the uncoordinated oxygen atom of the carboxyl group (Figure 4b); in consequence, this complex stabilizes by about 30 kJ/mol. For the various carboxylates examined, this rearrangement resulted in longer U-O_c bonds, by 0.08 Å longer on average, and shorter U-C distances, by about 0.06 Å (Table 4). Overall this improvement of the models does not lead to better agreement with experiment. U-carboxylate distances are still ~0.1 Å too short and the average U-O_{eq} changes at most ~0.01 Å (Table 4) [59,60].

We examined the effect of hydrolysis on uranyl monocarboxylate complexes for the bidentate complexes $[UO_2(OOCR)(OH)(H_2O)_2]$ of formiate, acetate, and propionate [60]. Due to the strong binding of the hydroxyl ligand, the U-O_t distance elongates to 1.80–1.81 Å. Bond competition also results in an elongation of the U-O_c bonds, by ~0.07 Å, which brings them close to the experimental findings (Table 3). Also the aqua ligand bonds are weakened. For the hydroxo-carboxylates, they are about 0.04 Å longer than typical EXAFS results (Table 3). Still, the deviation between experiment and computational results for U-O_{eq} remains. The calculated value, 2.38 Å, of U-O_{eq} in all species examined is nearly the same as for all other complexes inspected (Table 3). In summary, in the hydroxide complexes, the agreement with experiment improves for the parameters of the uranyl

Table 5. Geometric parameters (in Å) and symmetric uranyl stretching frequency ν_s (in cm^{-1}) of uranyl(VI) monoacetat $[UO_2(OOCCH_3)(H_2O)_n]^+$ in solution (PCM) with bi- and monodentate acetate coordination for the equatorial coordination numbers N = 5 and 6. Comparison with experimental results (Exp.) from solution (Sol.) and cyrstal structures (Cryst.). For the designations of the atoms, see Figure 3.

	n	N	U=O_t	U-O_c	U-C	U-O_w	U-O_{eq}	ν_s
bi	3	5	1.787	2.371	2.772	2.365	2.367	854
	4	6	1.787	2.400	2.783	2.462	2.441	846
	Exp.	CH_3 Solv.[a]	1.78(1)	2.50(2)	2.91(2)	2.38(2)	2.43(2)	861
		Sol.[b]	1.78(1)	2.46(4)	2.87(4)	2.40(4)	2.42(4)	–
		Cryst.[c]	1.76(3)	2.48(5)	2.86(5)	2.36(4)	2.42(6)	–
mono	4	5	1.789	2.291	3.401	2.382	2.364	824
	5	6	1.790	2.363	3.389	2.465	2.448	838
	Exp.	Sol.[b]	1.78(1)	–	–	–	2.38(4)	–
		Cryst.[c]	1.76(3)	2.39(5)	3.5(1)	2.42(6)	2.36(2)	–

[a] Refs. 30,69,70. [b] Average of data from Refs. 29-31. [c] Average of data from Refs. 10, 30, 71.

carboxylate bonds, but all other parameters agree less well with experiment. Especially the longer uranyl bond is noteworthy. Thus, we excluded hydrolysis as reason for the observed disagreement with experiment. As most experiments were performed at rather low pH, the presence of a ternary hydroxo carboxylate complexes has to be regarded anyhow as improbable [29,30].

The most common equatorial coordination number of uranyl complexes is N = 5 [29,64]. As coordination numbers are determined in EXAFS with an uncertainty of up to 20% [29, 30,67], neighboring coordination numbers N of 4 or 6 can not be excluded. Therefore, we also investigated the effect of coordination number N = 6 of equatorial ligands for the example of uranyl monoacetate [60,68] (Table 5, Figure 4). Due to bond competition with an additional aqua ligand, all equatorial bonds elongate. While uranyl-carboxylate distances are closer to the experimental data for N = 6 than for N = 5, the aqua ligand bond is slightly overestimated for N = 6. The weaker bonds of aqua ligands leads to a network of hydrogen bonds between them (Figure 4c,d). Interestingly, with the coordination number also the average equatorial uranyl-oxygen distance U-O_{eq} increases to ~2.44 Å for mono- and bidentate coordinated complexes. This value is close to the experimental result of ~2.42 Å (Table 5), which is regarded as indicative for bidentate coordination. According to our studies, the equatorial coordination number N is the only parameter which appreciably affects the value of U-O_{eq}. Therefore, we suggested a re-interpretation of the EXAFS results [59,60,68]. Accordingly, changes in the average equatorial uranyl-oxygen

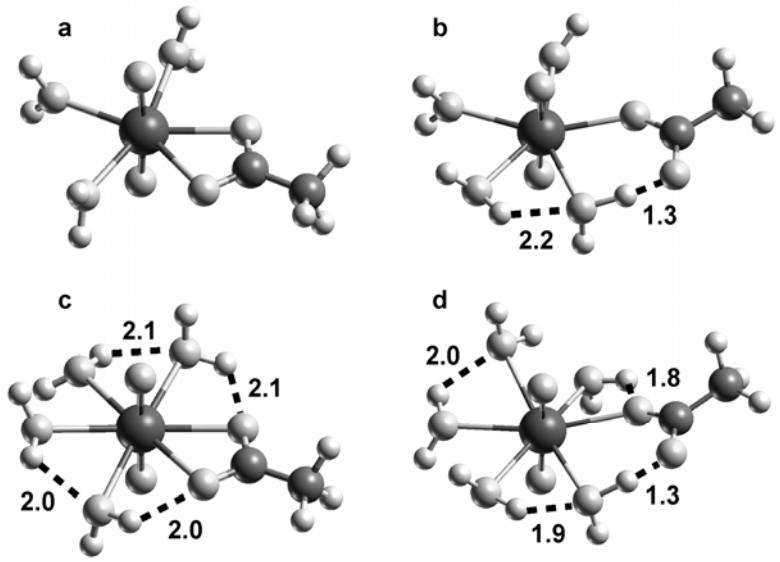

Figure. 4. Structures of uranyl(VI) monoacetate $[UO_2(OOCCH_3)(H_2O)_n]^+$, optimized without symmetry constraints, with different acetate coordination modes and equatorial coordination numbers N of uranyl : (a) N = 5, bidentate, (b) N = 5, monodentate, (c) N = 6, bidentate, (d) N = 6, monodentate. Dashed lines indicate hydrogen bonds, lengths in Å.

distance should be interpreted as a change of the coordination number, where values of ~2.37 Å are typical for N = 5, whereas U-O_{eq} values of ~2.44 Å indicate N = 6. This interpretation is supported by data from crystal structures, which formed the basis of the earlier interpretation which yielded an average U-O value of 2.38±0.05 Å for monodentate carboxylate groups and 2.48±0.05 Å for groups bound in bidentate fashion [10]. A re-evaluation of the *same* data according to the coordination numbers of the uranyl centers furnished U-O_{eq} values of 2.39 ±0.04 Å for N = 5 and 2.48±0.03 Å for N = 6, in line with our new interpretation. An average equatorial U-O distance which essentially only depends on the coordination number was also found for other complexes (Sections 4.2, 4.3). This finding is also important for the interpretation of EXAFS results on actinyl humate complexes (Section 4.4).

In the course of optimization of the various complexes discussed above, we also obtained thermodynamic parameters (Table 6). We characterized the stability of the complexes by a reaction where one (monodenate) or two (bidentate) aqua ligands are substituted by a carboxylate. For C_s symmetric model complexes, we calculated the same ligand exchange energy for both monodentate and bidentate forms of the monocarboxylates. Thus, the second uranyl carboxylate bond in bidentate complexes stabilizes the complex by about the same amount as an aqua ligand; for $UO_2(H_2O)_5^{2+}$, that energy is 80 kJ/mol on average [60]. Full geometry optimization revealed that monodentate complexes are about 30 kJ/mol more stable than bidentate complexes. We traced this back to a bridging hydrogen bond between an aqua ligand and the carboxyl group (see above). The trend of enthalpies is

Table 6. Calculated thermodynamic quantities of uranyl complexation by carboxylate due to a ligand exchange reaction:[a] energies ΔE_{sub}, enthalpies ΔH_{sub}, and free energies ΔG_{sub} (in kJ mol^{-1}) for complexes $[UO_2(OOCR)(H_2O)_n]^+$ with bi- (bi, n = 3) and monodentate (mono, n = 4) coordination. Calculations without symmetry constraints in the gas phase (GP) and in aqueous solution (PCM) .

	R	ΔE_{sub}		ΔH_{sub}		ΔG_{sub}	
		GP	PCM	GP	PCM	GP	PCM
bi	H	-832	-72	-839	-79	-867	-107
	CH_3	-861	-91	-868	-98	-902	-132
	CH_2CH_3	-859	-91	-861	-93	-901	-133
mono	H	-901	-110	-905	-114	-896	-104
	CH_3	-926	-121	-930	-125	-916	-111
	CH_2CH_3	-921	-122	-921	-123	-910	-112

[a] Reaction $[UO_2(H_2O)_5]^{2+} + [RCOO]^- \rightarrow [UO_2(OOCR)(H_2O)_n]^+ + (5–n)\ H_2O$

similar (Table 6). In contrast, when free energies are considered, bidentate complexation in solution is preferred by ~20 kJ/mol. This entropy effect reflects the release of two aqua ligands when a bidentate complex of the solvated uranyl is formed, while in the case of monodentate ligation only one aqua ligand is replaced. Comparison with corresponding free energies for models in the gas phase shows that only in solution this entropy effect is strong enough to reverse the stability of mono- and bidentate complexes (Table 6). Thus, the preference for bidentate complexation is the combined effect of solvation and entropy, in agreement with experimental findings for many crystal structures and the structure of uranyl triacetate.

Neptunyl monocarboxylates

We examined monocarboxylates of the most stable oxidation state V of neptunyl and of NpO_2^{2+} and we compared them to analogous complexes of uranyl(VI) [60]. We employed the same model approach as for uranyl (see above). As expected, we obtained rather similar results for neptunyl(VI) while for neptunyl(V), due to the lower charge, we obtained less stable complexes. For neptunyl(VI), the neptunyl bond and the bonds to the ligands were determined 0.02 Å shorter than for their uranium congeners (Table 7). This reflects the smaller radius of the neptunyl ion for the same oxidation state (actinide contraction [64]). The additional f electron of neptunyl(VI) is only marginally involved in ligand bonding. Thus, uranyl and neptunyl(VI) complexes yield also rather similar ligand exchange energies. For all complexes and coordination modes examined (Table 7), the reaction energies differ less than 5 kJ/mol.

Table 7. Geometric parameters (in Å) and symmetric neptunyl stretching frequency ν_s in cm^{-1} for neptunyl(V) monocarboxylates $[NpO_2(OOCR)(H_2O)_n]$ in solution (PCM) with bi- (bi, n = 3) and monodentate (mono, n = 4) carboxylate coordination in comparison to experimental data from cyrstal structures (Cryst.) Comparison of average values (Av.) of for Np(V), Np(VI), and U(VI) complexes for different residues R. ΔNp(VI) = values of Np(V) minus values of Np(VI). Designation of the atoms in analogy to Figure 3.

	R	Np=O_t	Np-O_c	Np-C	Np-O_w	Np-O_{eq}	ν_s
bi	H	1.818	2.470	2.822	2.408	2.433	771
	CH_3	1.821	2.445	2.819	2.417	2.428	770
	CH_2CH_3	1.830	2.441	2.815	2.449	2.446	778
Exp.	Np(V) Cryst.[a]	1.85(3)	2.59(8)	2.94(4)	2.47(7)	2.55(2)	–
	Np(V) Av.	1.82	2.45	2.82	2.42	2.42	773
	Np(VI) Av.	1.77	2.36	2.75	2.34	2.35	888
	U(VI) Av.	1.79	2.38	2.77	2.36	2.37	857
	ΔNp(VI)	0.05	0.09	0.07	0.08	0.07	-115
	CH_3	1.822	2.310	3.446	2.457	2.428	769
	CH_2CH_3	1.822	2.316	3.451	2.459	2.430	769
Exp.	Np(V) Cryst.[a]	1.84(2)	2.45(2)	–	2.47(7)	2.47(2)	–
	Np(V) Av.	1.82	2.32	3.45	2.46	2.43	770
	Np(VI) Av.	1.77	2.18	3.38	2.40	2.36	850
	U(VI) Av.	1.79	2.21	3.40	2.42	2.38	848
	ΔNp(VI)	0.05	0.14	0.07	0.06	0.07	-80

[a] Ref. 13.

For monocarboxylate complexes of neptunyl(V), we calculated considerably longer bond distances (Table 7). Compared to oxidation state VI, the neptunyl bond is 0.05 Å longer and the bonds to the carboxyl oxygen atoms increase by ~0.1 Å for bidentate and ~0.15 Å for monodentate carboxylates. As for uranyl, the average equatorial Np(V)-O distance is independent of the coordination mode and amounts to 2.43 Å for five-fold neptunyl coordination. Evaluation of crystal structures again suggested a longer Np-O_{eq} distance for bidentate compared to monodentate carboxylate binding [13]. As for uranyl, we suggested also for neptunyl complexes in solution that the value of Np-O_{eq} should mainly be determined by the coordination number [60].

Exchange energies of aqua ligands by a carboxylate ligand are ~60 kJ/mol smaller for neptunyl(V) than for neptunyl(VI). For neptunyl(V), in contrast to uranyl(VI), bidentate coordination of the carboxyl group was calculated to be already energetically slightly favored. The two f electrons of neptunyl(V) are not strongly involved in the ligand interaction and remain mainly localized on the Np center. Correspondingly, triplet states

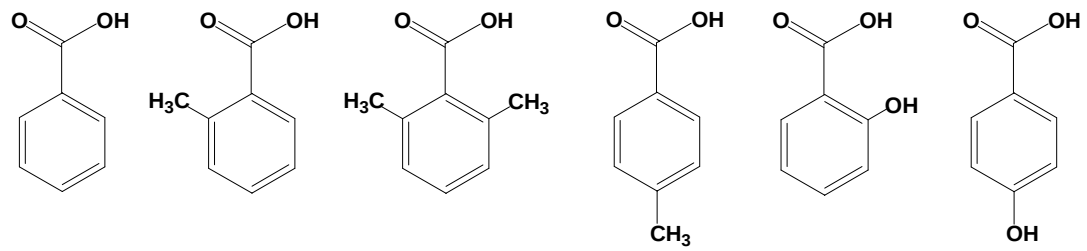

Figure 6. Sketches of aromatic carboxylic acids inspected as ligands in uranyl monocarboxylate: Benzoic acid, methyl and hydroxyl substituents.

were calculated to be more stable than singlet states, by ~40 kJ/mol for bidentate complexes and ~20 kJ/mol for monodentate complexes [60].

4.2 Complexes with aromatic carboxyl ligands

We examined aromatic carboxylic acids as ligands of uranyl by means of five-coordinate monocarboxylate model complexes [73] – in the same way as complexes of aliphatic ligands (see above). Benzoic acid as well as methyl and hydroxyl substituents (Figure 6) served as models of carboxylic groups attached to aromatic rings in humic substances and thus helped to complement the results for their aliphatic congeners. Para substituents of benzoic acid may be viewed as models of aromatic rings that are connected to a larger organic framework. Ortho substituents may be taken to represent steric and electrostatic effects of different chemical environments of carboxylic groups at aromatic rings.

Table 8 collects the calculated results for interatomic distances, energies and free energies of the exchange of aqua ligands by carboxyl. Uranyl monobenzoate yielded very similar results as acetate. As an effect of the polarizability of the aromatic ring, we noted slightly lower complexation energies (by ~10 kJ/mol), in line with the trend to lower pK_a values of aromatic acids compared to small aliphatic ones.

Substitution in para position had a very small effect on geometric parameters; they changed by less than 0.02 Å. Also energies were comparable; they increased by a few kJ/mol (Table 8). Interestingly, there again is no difference in $U\text{-}O_{eq}$ values between mono- and bidentate complexes, irrespective of the systems considered. This nicely corroborates our previous conclusion that this geometric parameter is independent of the coordination mode. The results for para-substituted benzoic acids also confirmed that small molecular models of the size inspected seem to be sufficient for representing carboxylic sites of larger organic molecules. A carboxylic group connected to a polyaromatic framework is an interesting case, yet to be examined, which may furnish larger changes.

Effects of substituents on bidentate uranyl monocarboxylate complexes turned out to be negligible (Table 8). The small increase in the ligand substitution energy noted for para substituents is also present for a methyl subsitutent in ortho position of the aromatic ring.

Tabelle 8. Uranyl monocarboxylates $[UO_2OOCR(H_2O)_n]^{2+}$ of benzoic acid and substituents (Figure 6) in solution (PCM) with bidentate (bi, n =3) and monodentate (mono, n = 4) coordination of the carboxyl group. Comparison of geometric parameters (in Å), ligand substitution energies and free energies[a] (in kJ/mol).

	R	U=O_t	U-O_c	U-C	U-O_w	U-O_{eq}	ΔE	ΔG
bi	C_6H_5	1.785	2.37	2.77	2.36	2.37	-83	-125
	C_6H_4(p-CH_3)	1.786	2.37	2.76	2.37	2.37	-86	-128
	C_6H_4(p-OH)	1.787	2.37	2.77	2.37	2.37	-90	-133
	C_6H_4(o-CH_3)	1.787	2.36	2.77	2.37	2.37	-88	-125
	C_6H_4(o-CH_3)$_2$	1.788	2.36	2.77	2.37	2.37	-75	-115
	C_6H_4(o-OH)	1.783	2.39	2.80	2.35	2.37	-36	-100
	CH_3	1.786	2.37	2.77	2.37	2.37	-91	-132
mono	C_6H_5	1.788	2.27	3.31	2.39	2.37	-111	-99
	C_6H_4(p-CH_3)	1.788	2.29	3.29	2.39	2.37	-115	-105
	C_6H_4(p-OH)	1.789	2.27	3.34	2.39	2.37	-118	-103
	C_6H_4(o-CH_3) syn	1.789	2.30	3.34	2.38	2.36	-112	-96
	C_6H_4(o-CH_3) anti	1.790	2.26	3.35	2.39	2.37	-112	-100
	C_6H_4(o-CH_3)$_2$	1.788	2.29	3.34	2.38	2.37	-95	-77
	C_6H_4(o-OH) syn	1.786	2.32	3.38	2.38	2.37	-74	-52
	C_6H_4(o-OH) anti	1.788	2.27	3.38	2.39	2.36	-81	-66
	CH_3	1.789	2.29	3.35	2.38	2.36	-121	-111

[a] Reaction $[UO_2(H_2O)_5]^{2+} + [RCOO]^- \rightarrow [UO_2(OOCR)(H_2O)_n]^+ + (5–n)\ H_2O$

For the di-ortho methyl derivative this trend is reversed and the free energy of ligand substitution is even 10 kJ/mol smaller than for benzoate. The substitution energies of the ortho hydroxyl species are even smaller; this can be rationalized via the stabilization of the anionic ligand by a hydrogen bond between the carboxyl and hydroxyl groups. Concomitantly, we calculated a slightly shorter uranyl bond and 0.03 Å longer distances U-O_c and U-C to the carboxyl group.

For monodentate carboxylate coordination, we determined stronger variations with the type of the substitutent. For ortho hydroxyl species, we noted distinct effects of the position of the hydroxyl group – syn or anti with respect to the uranyl carboxylate bond. Structures of “anti” configurations are very similar to that of the simple monodentate benzoate complex. For syn position of the hydroxyl group, the value of U-O_c is 0.05 Å larger and the binding of the ligand to uranyl is weaker. A methyl substituent has a similar, but weaker effect. As for the bidentate coordination mode, we noted a destabilization of the monodentate complex for di-ortho methyl benzoate. Due to the emerging sixfold ring, chelate complexes by ortho hydroxyl benzoate were less favorable than the examples discussed thus far.

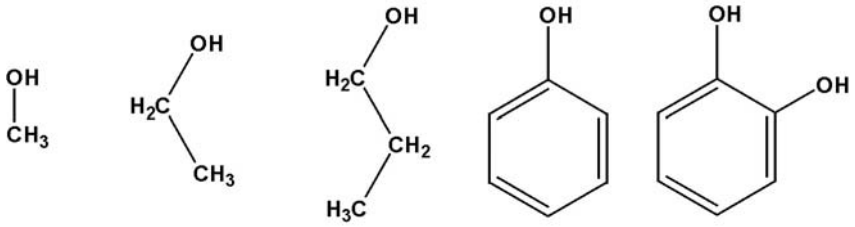

Figure 7. Alcohol ligands examined in uranyl mono-alcohol and -alcoholate complexes: methanol, ethanol, propanol, phenol, and catechol.

Overall, carboxyl groups attached to aromatic rings are slightly weaker bound than aliphatic carboxylates. The corresponding ligand substitution energies varied more. Therefore, analogous functional groups of humic substances are expected to provide a range of weaker complexation sites compared to aliphatic carboxyl groups.

4.3 Complexes with alcohol ligands

Experiments at pH 4, where phenolic hydroxyl groups were blocked by methylation, revealed that the loading capacity of humic acids in uranyl complexation decreases [74]; this finding was taken to indicate a contribution of these groups in uranyl complexation. A similar result was obtained for Np(V) [75]. In contrast, EXAFS experiments at pH 2 did not reveal any change compared to unmodified humic acids [76]. These experiments of the project partner Institute of Radiochemistry at the Forschungszentrum Dresden-Rossendorf represent a very rare case where functional groups of humic substances other than carboxyl have been studied with regard to actinide complexation. They stimulated our related computational model study [77]. This comparison of carboxylic and alcoholic mono-ligand complexes also broadened the range of functional sites examined in the present project

We modeled complexes of uranyl(VI) with single methanol, ethanol, propanol, phenol, and catechol ligands (Figure 7), following the strategy as for carboxylic acids [77]. We considered protonated as well as deprotonated alcohol ligands to inspect the interaction of uranyl in different pH regimes (Table 9). For deprotonated alcohol ligands, referring to a high pH regime, we noted a strong interaction between uranyl and the alcoholat ligand in uranyl(VI) monoalcoholates. The uranyl bond of 1.80–1.81 Å is up to 0.02 Å longer than that of carboxylates, e.g. acetate (Table 9). Correspondingly, we determined rather short U-O_c bonds of 2.1–2.2 Å, which are comparable to U-O bonds of hydroxide or monodentate carboxylates. For protonated alcohol ligands, which are to be expected at low pH, a shorter uranyl bond of 1.78 Å was calculated and the U-O_c bonds were typically between 2.3 and 2.4 Å (Table 9). The U-C distance, often determined by EXAFS experiment as a helpful quantity to distinguish different complexation modes, turned out to be less characteristic. Typical values were around 3.4 Å, with a tendency to lower values for deprotonated and higher values for protonated alcohols. As for the carboxylate ligands, we did not observe

Table 9. Calculated structural parameters, (distances in Å, angles in degrees) for complexes $UO_2(H_2O)_4OR]^+$ and $[UO_2(H_2O)_4HOR]^{2+}$ of uranyl with alcohols, optimized without symmetry constraints in solution (PCM). Complexes with H_2O and OH^- ligands (R = H) as well acetate are also shown.

	R	U=O	U-O_c	U-C	U-O_{eq}	ν_s
OR^-	H	1.795	2.20		2.37	834
	CH_3	1.807	2.09	3.24	2.37	795
	CH_2CH_3	1.807	2.08	3.45	2.37	800
	$CH_2CH_2CH_3$	1.807	2.08	3.46	2.37	814
	C_6H_5	1.798	2.17	3.33	2.37	826
	2-OH-C_6H_4 anti[a]	1.798	2.14	3.45	2.37	867
	2-OH-C_6H_4 syn[a]	1.800	2.13	3.45	2.38	
CH_3COO^-		1.790	2.20	3.40	2.38	846
HOR	H	1.781			2.36	869
	CH_3	1.778	2.34	3.41	2.36	854
	CH_2CH_3	1.782	2.34	3.40	2.36	835
	$CH_2CH_2CH_3$	1.778	2.32	3.45	2.38	
	C_6H_5	1.777	2.46	3.53	2.38	853
	2-OH-C_6H_4 anti[a]	1.777	2.50	3.77	2.39	
CH_3COOH		1.790	2.20	3.40	2.38	846
Exp. Sol.[b]		1.78(2)			2.39(2)	

[a] H of second hydroxyl group oriented syn or anti with respect to first hydroxyl group
[b] Ref. [17].

any effect of the type of complex on the average U-O_{eq} distance. The calculated values, all close to 2.37 Å, compare very well with the results for carboxylates (Tables 3 and 8) and reflect the same coordination number of 5, chosen for these model complexes. The close similarity of geometric parameters U=O_t and U-O_{eq} for alcoholate ligands and carboxyl groups nicely rationalizes the agreement of EXAFS results for uranyl complexation with unmodified and blocked humic acids at pH 2 [76]. Thus, these parameters are not suited for discriminating between hydroxyl or carboxyl sites; alcoholic groups have to be expected to contribute to uranyl complexation.

We calculated the energy of complexation of uranyl by alcohols and used protonated alcohols and alcoholate complexes as references as this corresponds to typically low pH at which uranyl complexation by humic acids is experimentally examined (Table 10) [74,76]. To gain a better understanding, the reaction is divided into two steps, deprotonation and complexation (Figure 8). Two pathways to uranyl alcoholates can be envisaged. First the alcohol may deprotonate, depending on pH, and then replace an aqua ligand at the uranyl

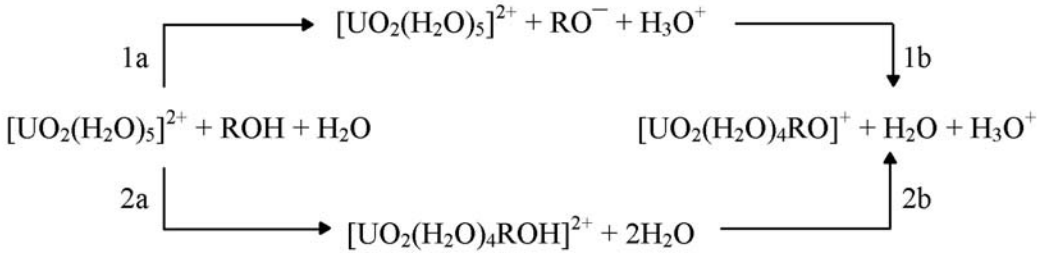

Figure 8. Reaction scheme for the complexation of solvated uranyl by an alcohol ligand. Path 1: deportonation of the alcohol with subsequent uranyl complexation. Path 2: uranyl complexation with subsequent deprotonation of the alcohol.

ion (Path 1). Alternatively, first the alcohol may complexate with uranyl and deprotonate in a second step in the field of the uranyl ion (Path 2).

Inspection of Table 10 shows that deprotonation of aliphatic and phenolic alcohols is strongly endothermic (1a). The deprotonation energy qualitatively correlates with the pK_a values; this includes even complexation by an aqua ligand or acetic acid. We determined the same approximate correlation for the exothermic step of complexation of uranyl by the alcoholate (1b), where phenol and catechol yield rather small free energies, comparable to acetate (Table 10).

In summary, one notes a trend where aromatic alcohols show similar total reaction energies than aliphatic ones. Path 2 starts with the attachment of the alcohol to uranyl, which is slightly exothermic for aliphatic, but endothermic for aromatic alcohols. The deprotonation energy of alcohols in the field of uranyl is considerably reduced compared to free alcohols. Overall, Path 2 avoids the high barrier of alcohol deprotonation and thus can be regarded as the preferred route of uranyl complexation by alcohols.

Table 10. Total free energy ΔG_{tot} (in kJ/mol) and free energies of partial steps 1a, 1b, 2a, and 2b of the reaction of uranyl(VI) with an alcohol ligand to form $[UO_2(H_2O)_4OR]^+$ in solution according to the reaction scheme of Figure 8. Analogous values for the complexation of uranyl by acetate and hydroxide (R = H) are shown for comparison.

R	1a	1b	2a	2b	ΔG_{tot}
H	317	-271	0	46	46
CH_3	264	-234	-17	47	30
CH_2CH_3	260	-215	-7	52	45
$CH_2CH_2CH_3$	258	-198			60
C_6H_5	172	-114	47	11	58
(2-OH)C_6H_4 anti	180	-125	32	23	55
CH_3COOH	150	-117	10	23	33

Table 11. EXAFS data (distances in Å) for the complexation of uranyl(VI) and neptunyl(V) by natural and synthetic humic acids (HA), compared with averaged data from crystal structures of actinyl carboxylates. The crystal structure data provide distances An-O_{eq} averaged over complexes with a given equatorial coordination number N = 5 or N = 6) and An-O_c for a given coordination mode of the carboxylate ligand (monodentate and bidentate). For the designations of the atoms, see Figure 3.

		An=O_t	An-O_{eq}	An-O_c
U(VI)-HA[a]		1.77–1.78	2.37–2.39	–
Cryst.[b]	N = 5	1.76±0.03	2.39±0.02	
	N = 6	1.74±0.04	2.48±0.02	
	mono	1.76±0.03		2.39±0.05
	bi	1.76±0.03		2.48±0.05
Np(V)-HA[c]		1.84–1.85	2.48–2.49	–
Cryst.[d]	N = 5	1.85±0.03	2.45±0.03	
	N = 6	1.85±0.03	2.55±0.03	
	mono	1.85±0.03		2.46±0.04
	bi	1.85±0.03		2.59±0.08

[a] EXAFS data from solution, Refs. 10,15. [b] Averaged values from crystal structures, Ref. 10. [c] EXAFS data from solution, Ref. 13. [d] Averaged values from crystal structures, Ref. 13.

4.4 Remarks on actinyl complexation by humic acids

Actinyl complexation by humic acids at low pH is expected to take place mainly via carboxylic groups [3,6,7,10,13,15] with some contribution of phenolic groups [74,75], especially at higher pH values. Consequently, EXAFS data on the structure of actinyl humate complexes have been interpreted using carboxylate crystal structures as reference [12,13,15]. From short U-O_{eq} values of ~2.38 Å for uranyl(VI) and ~2.48 Å for neptunyl(VI) as well as missing signals of U-C distances, a monodentate uranyl humate complex structure was inferred [12,13], whereas longer values, by ~0.05 Å, would have been expected for bidentate coordination [10,13,30,71]. EXAFS experiments on Np(IV) arrived at similar results [22]. This interpretation is mainly based on An-O_c distances from crystal structures (Table 11), assuming that U bonds to aqua ligands are rather independent of the coordination mode of the carboxyl group [12].

As discussed in the previous sections, we examined computationally complexes of uranyl and neptunyl with one carboxylate ligand and we took them to represent carboxylate groups of humic substances. As a most remarkable result, we noted that the average bond length between uranyl and oxygen donor ligands does not depend on the coordination mode for monocarboxylates, in contrast to experimental results inferred from crystal structures

Table 12. Comparison of calculated geometrical parameters (in Å) of uranyl(VI) complexes $UO_2X(H_2O)_n$, where X are carboxylates, alcohols, alcoholates, or hydroxides, for coordination numbers N = 4–6 in the equatorial plane of uranyl as well as for various coordination modes (Coord.). Except in the pseudo-bridging structure of acetate, models with C_s symmetry constraints were examined. For the designations of the atoms, see Figure 3.

X	Coord.	n	N	U=O_t	U-O_x	U-O_w	U-O_{eq}
$(OH)_2^{2-}$	–	2	4	1.82	2.14	2.47	2.31
–	–	4	4	1.77	–	2.31	2.31
OH^-	–	4	5	1.80	2.10	2.44	2.37
CH_3COO^-	bi	3	5	1.79	2.37	2.36	2.36
	mono	4	5	1.79	2.20	2.42	2.38
	pseudo	4	5	1.79	2.29	2.38	2.36
$CH_2(OH)COO^-$	chelate	3	5	1.79	2.33	2.38	2.36
$(CH_3COO)_2^{2-}$	bi	1	5	1.79	2.38	2.35	2.37
$OH(CH_3COO)^{2-}$	bi	2	5	1.81	2.12/2.44[a]	2.44	2.38
$OH(C_2H_5COO)^{2-}$	bi	2	5	1.81	2.12/2.44[a]	2.44	2.38
CH_3O^-	–	4	5	1.81	2.07	2.45	2.38
$C_6H_5O^-$	–	4	5	1.80	2.13	2.44	2.38
CH_3OH	–	4	5	1.78	2.41	2.37	2.38
C_6H_5OH	–	4	5	1.78	2.42	2.36	2.37
–	–	5	5	1.78	–	2.36	2.36
$(CH_3COO)^-$	bi	4	6	1.79	2.39	2.46	2.44
$(CH_3COO)_2^{2-}$	bi	2	6	1.79	2.42	2.49	2.45
$(CH_3COO)_3^{3-}$	bi	0	6	1.80	2.42	–	2.42
–	–	6	6	1.79	–	2.41	2.41

[a] Short bonds refer to hydroxide, longer ones to carboxylate.

(Table 11). Assuming coordination number N = 5 for uranyl, the value most often encountered, we calculated an almost constant value for U-O_{eq} of about 2.37±0.02 Å for various carboxylic acids and different complexation modes (Tables 3 and 8). We also obtained very similar values for monoligated complexes with alcohols and alcoholates (Table 9).

Extending the discussion for the exemplary case of acetate (Section 4.1), we collected in Table 12 calculated structural characteristics of typical carboxyl and alcohol complexes, also with different coordination numbers N, and compared them to results for solvated uranyl (aqua ligands only) and hydroxides as well as ternary complexes (hydroxo-carboxylates). All these data were determined with the same computational procedure. Inspection of Table 12 confirms that the values of U-O_{eq} are mainly determined by the coordination number N of the complexes, but are essentially independent of the type of

ligand and its coordination mode. This interpretation is also in line with crystal structure data as an evaluation of crystal structures with respect to the coordination number of the actinyl ion demonstrates: coordination number N = 5 yields shorter An-O_{eq} values then N = 6 (Table 11).

On the basis of these findings, we suggest a reinterpretation of pertinent EXAFS results to indicate five-fold coordination of uranyl humate complexes instead of mono-dentate complex structures. Unfortunately, the complexation mode as well as the number of functional groups involved can not be inferred from the indicator U-O_{eq} only. Thus, a separation of different bond distances in the first ligand shell, an identification of the U-C distance or help from other spectroscopies is needed to gain more detailed insight in the nature of actinyl humate complexes.

As carboxylates in general prefer bidentate coordination [78], one can also expect a bidentate coordination mode for actinyl humates. Our calculations support this expectation: bidentate coordination is preferred as an entropy effect (Sections 4.1, 4.2). An open issue is the role of chelate complexes. In this project, we studied only a few examples, invoking models with C_s symmetry constraints. For glycolate, salicylic acid, as well as catechol, these estimates did not yield any energetic preference compared to bidentate carboxylate com-plexes [73,77]. Yet, one can not exclude that particular combinations of functional groups exist, which form strong coordination bonds via a chelate ring. On the other hand, due to specific structural requirements, these sites should be rare and thus should not be of determining influence on actinyl complexation by humic acids.

Given our results for aliphatic carboxylates of increasing chain length as well as the small calculated substituent effects for aliphatic and aromatic carboxylic acids, we refrained from inspecting larger models of humic acid sites because only small corrections of our model results had to be expected. Instead, in view of the experience gained in this project, we regarded the treatment of solvation as a more important issue, worth further studies which should aim at improving and confirming the present results (see Section 4.6).

4.5 Thermochemistry of actinyl ions

In this project we also showed that modern quantum chemistry methods are very useful for determining fundamental thermochemical data for actinide compounds, for which in some cases only experimental data of limited accuracy exist [79]. In a showcase fashion, we demonstrated this for the enthalpy of formation of uranyl(VI) [79] and plutonyl(VI) [80]. For this purpose, we selected a series of formal reactions which transform actinyls into species for which the enthalpies of formation are known with good accuracy. The enthalpies of formation were obtained via calculated reaction enthalpies and known (experimental) formation enthalpies of all other species involved. Using the BP XC functional, we determined $\Delta_f H^\circ_0$ at 1527±42 kJ/mol for uranyl(VI); with the PW91 XC functional, the

result was 1548±50 kJ/mol [79]. These values are in very good agreement with a new experimental determination, carried out simultaneously, which yielded $\Delta_f H^\circ_0$ = 1523±63 kJ/mol [81]. Thus, previous estimates of 1300 kJ/mol ≤ $\Delta_f H^\circ_0$ ≤ 1800 kJ/mol [82] and other earlier estimates were significantly improved, in line with this recent, more accurate experiment [81]. In the same way, the enthalpy of formation for PuO_2^{2+} was calculated at $\Delta_f H^\circ_0$ = 1749±63 kJ/mol via model reactions involving plutonium fluorides [80]. Also this result agreed very well with a very recent experimental result, $\Delta_f H^\circ_0$ = 1728±67 kJ/mol [81] which relied on new measurements of the ionization potentials of PuO_2 und PuO_2^+. To reach such accurate computational results, both these computational studies employed relativistic density functional methods that included a new self-consistent treatment of the spin-orbit interaction developed in our group (see below) [83,84].

4.6 Methodological topics

Relativistic treatment of the Coulomb interaction of electrons

As stated earlier, all electronic structure calculations of this project were carried out with the Douglas-Kroll-Hess approach [38] to relativistic density functional theory [32,33]. The parallel density functional software PARAGAUSS [34], developed in our group, affords a very efficient scalar relativistic method to solve the Kohn-Sham-Dirac problem at the all-electron level as well as several variants that permit a self-consistent treatment of spin-orbit interaction [32,33]. The more accurate variants, which include spin-orbit interaction, are mainly important for treating open-shell complexes as well as for spectroscopic studies, but are also very useful for the accurate determination of thermodynamic parameters of actinide complexes (see above) [79,80].

For most applications, also of this project, the more economic scalar relativistic approximation suffices where only two terms of the electronic Hamiltonian, the kinetic energy and the Coulomb potential of the nuclei, are subject to a relativistic transformation [32,38]. The terms of electron-electron interaction are kept in their non-relativistic form. The nuclear potential of the electrons accounts for the largest part of the spin-orbit interaction; we had suggested such a method some years ago [85]. In a preceding project (BMWi 02E9450), we developed a self-consistent relativistic treatment of spin-orbit interaction that, in addition, takes the Hartree part of the electron-electron interaction into account. It relies on a matrix representation of the relevant operator products in momentum space [86]. This numerical approach requires very flexible basis sets and entails a considerable computational effort. During this project, we introduced a new algorithm, which is more accurate, numerically more stable, and more efficient. This new approach relies on a direct, analytic evaluation of the matrix representation of the relativistic Hartree term [84]. In addition, basis sets of normal size suffice and thus result in an improved computational efficiency [84]. For dimer molecules with heavy elements, we demonstrated these advantages of the new approach. This methodological advance considerably facilitates inclusion of spin-orbit

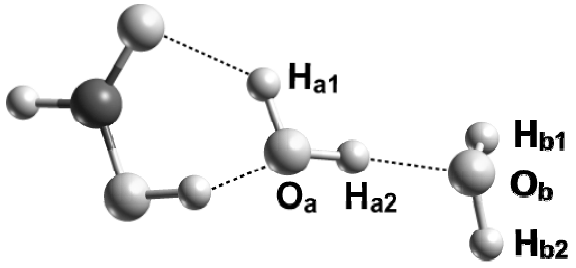

Figure 10. Model system $HCOOH(H_2O)_2$ to probe the interaction of a carboxylic acid with the solvent molecules. One aqua ligand H_2O_a positioned in the first solvation shell, the other, H_2O_b, in the second solvation shell.

interaction in accurate calculations. This new method will be very valuable for applications in actinide chemistry, e.g. when low oxidation states of actinides have to be treated [79,80], as envisaged in a subsequent project.

A discrete QM/MM solvation model

In this project, solvation of complexes in an aqueous solution was described with a two-step procedure. The first solvation shell of actinyl complexes was explicitly included in that part of the model that was treated at the quantum mechanical level. In addition, long-range solvation effects of the remaining solvent environment were accounted for via a polarizable continuum model (PCM, Section 3). Thus, beyond the first solvation shell, the discrete nature of the solvent was neglected. Recently, calculations which included explicit water molecules of the second shell showed that chemical effects like charge transfer may occur in this part of a system, which are not represented by a PCM treatment [48-50] (Section 3). Especially for highly charged ions and in situations where the orientation of aqua ligands in a complex plays a key role, e.g. in pseudo-bridging structures of actinyl monocarboxylate complexes (Section 4.1), explicit modeling of the second solvation shell may lead to more accurate results.

Quantum mechanical modeling of actinide complexes that includes an extended shell of solvent molecules requires notably larger computational resources, especially during a geometry optimization. Therefore, we developed a QM/MM approach that combines quantum mechanical and molecular mechanical methods for different parts of a system [51,52, 87,88], to achieve an improved representation of the solvation environment. To account for the discrete nature of the solvent environment in an efficient way, the actinide complex itself and a limited number of solvent molecules are treated with a quantum mechanical method (QM region), while a shell of more distant solvent molecules is represented by a "classical" force field (MM region). We chose the well established family of TIPnP water models [89,90] to describe solvent molecules in the MM region. In these models, water molecules are considered as rigid with a fixed charge distribution [89,90]. Inclusion of polarization and charge transfer effects need more elaborate force fields, which will be

Table 13. Interaction of formic acid with aqua ligands: $HCOOH \cdot H_2O$ and $HCOOH \cdot (H_2O)_2$ with one aqua ligand positioned in the second shell (Figure 10). Quantum mechanical results for $HCOOH \cdot H_2O$ (n=1) and effect Δ of the second-shell aqua ligand (n = 2) from quantum mechanical (ΔQM) and QM/MM calculations with TIPnP force fields (ΔTIP3P und ΔTIP4P) representing the water molecule in the second solvation shell. Distances in Å, angles in degree. For the designation of the atoms, see Figure 10.

$HCOOH \cdot (H_2O)_n$	n=1	n=2		
	QM	ΔQM	ΔTIP3P	ΔTIP4P
C=O	1.232	0.000	0.000	0.000
C-O	1.335	-0.002	-0.003	-0.003
O-H	1.022	0.016	0.016	0.014
$O \cdots HO_a$	1.895	0.173	0.128	0.075
$H \cdots O_a$	1.658	0.083	0.074	0.063
O_a- H_{a1}	0.994	-0.008	-0.006	-0.005
O_a- H_{a2}	0.975	0.018	0.028	0.020
COH	107	0.7	-0.3	-0.3
OCO	126	0.1	0.3	0.3
$H_{a1}O_aH_{a2}$	107	-0.2	-1.8	-0.7
OHO_a	157	5.7	4.7	3.7
OH_aO_a	140	-7.2	5.0	3.5

added at a later stage of development. The QM/MM approach implemented in the software PARAGAUSS [34] relies on the additive Hamitonian $H_{tot} = H_{QM} + H_{MM} + H_{int}$, where the coupling term H_{int} includes electrostatic and van der Waals interactions between the QM and MM regions of the system under study. A three-step procedure was also realized; in addition to the QM/MM partitions, it also includes a PCM representation of the farther environment. While the QM/MM method describes a solvated complex as a molecule in a water cluster, the extended QM/MM/PCM procedure also accounts for long-range electrostatic effects.

The method was validated and its performance was demonstrated by comparison with full density functional calculations for a series of test systems. Results for $(H_2O)_2$ and $(H_2O)_3$ showed that, in comparison to density functional calculations, a TIP4P model yields more accurate geometries than a TIP3P description. In QM/MM calculations of $(H_2O)_2$ where one of the water molecules is treated by the force field, more accurate results are expected if the donating molecule is assigned to the QM partition. In this case, the resulting length of the hydrogen bond deviates only 0.01 Å from the result of a full density functional optimization; a MM description of the donating molecule leads to a deviation of 0.08 Å. The binding energy of $(H_2O)_2$, 31 kJ/mol, and the solvation energy, 49 kJ/mol, as obtained

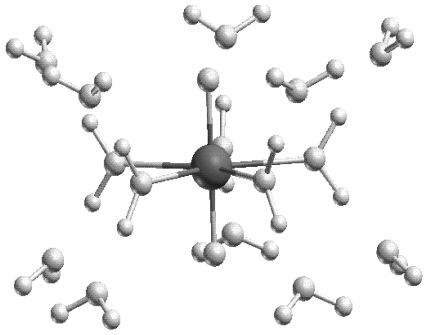

Figure 11. Model of the solvated uranyl ion in D_{5h} symmetry.

in a density functional reference calculation, are slightly underestimated with a QM/MM treatment. In the model with the donating water in the MM region, these deviations are 2 and 9 kJ/mol, respectively, whereas in the reversed model (accepting water molecule in the MM region) these deviations are less than 1 and 6 kJ/mol, respectively. To probe the effect of a solvent molecule of the second shell, we also studied a simple model of formic acid and two aqua ligands (Figure 10); there, one of the water molecules coordinates directly to formic acid, while the second one is only in contact with the first aqua ligand. From a full density functional optimization of this model complex, one identifies an elongation of the two hydrogen bonds between the acid and the solvent molecule of the first shell, by 0.17 and 0.08 Å (ΔQM, Table 13), as main effect of the second water molecule on $HCOOH{\cdot}H_2O$. In a QM/MM treatment, where the aqua ligand of the second shell is assigned to the MM part, these effects as well as smaller changes of the molecule are qualitatively well reproduced. With a single exception, also effects on bond angles are rather accurately modeled by the QM/MM procedure (Table 13). As a trend, the MM treatment of the outer solvent molecule results in a minor underestimation of second-shell effects; on average, the TIP3P model performs slightly better than the TIP4P force field.

To illustrate the three-step modeling of an extended solvation shell including embedding in a PCM model (QM/MM/PCM), we present results for a solvated uranyl(VI) ion where D_{5h} symmetry constraints have been invoked (Figure 11, Table 14). At the QM/MM level, when only the first solvation shell is explicitly treated in the model compound $UO_2^{2+}(H_2O)_5$, one notes strong structure relaxations from the full density functional result. The uranyl bond, 1.75 Å, is calculated 0.03 Å too short and the U-O_w bonds to the aqua ligands are underestimated by ~0.3 Å (Table 14). Addition of a second explicit solvation shell in the model complex $UO_2^{2+}(H_2O)_{15}$ has only small effects on the solvated uranyl ion; the uranyl bond U=O and the U-O_w bonds increase by ~0.01 Å. A QM/MM calculation with the second solvation shell represented by a force field yields very good agreement with the results from the full density functional calculation (Table 14), even though the second-shell solvent molecules are attached in donating configurations via hydrogen bonds to the first shell of aqua ligands. The uranyl bond U=O is underestimated

Table 14. Model of the solvated uranyl(VI) ion with D_{5h} symmetry constraints. Comparison of geometric parameters (distances in Å, angles in degree) from quantum mechanical (QM) and QM/MM calculations, including embedding in a PCM model. Uranyl bond U=O, uranyl water bond U-O_a, hydrogen bond H···O_b between first and second solvation shell, angle OUO_b between uranyl oxygen, uranium, and an oxygen center of an aqua ligand of the second shell. Aqua ligands of the first solvation shell are denoted as H_2O_a, of the second as H_2O_b. In QM/MM calculations, the outermost solvation shell of the complexes is represented by the TIP4P force field.

		U=O	U-O_a	H···O_b	OUO_b
$UO_2^{2+}\cdot(H_2O)_5$	QM	1.78	2.37		
	QM/MM	1.75	2.04		
$UO_2^{2+}\cdot(H_2O)_{15}$	QM	1.79	2.38	1.59	63.1
	QM/MM	1.77	2.39	1.62	63.2

by 0.02 Å, while the U-O_w bonds are well reproduced with deviations of only 0.01 Å. The hydrogen bonds H···O_b between the first and the second solvation shells reproduce the full quantum mechanical result within 0.03 Å (Table 14).

These results demonstrate that the QM/MM approach implemented is well suited for describing an extended explicit solvation environment of an actinide complex in a sufficiently accurate and efficient manner.

5 Summary and Outlook

Quantum mechanical modeling of actinyl complexation by humic substances was the central topic of the project. Humic substances, especially their soluble fraction, which comprises fulvic and humic acids, considerably affect the chemical state and the migration of actinide elements in the environment due to their complexating and redox abilities. In addition, their sorption on minerals and coagulation to immobile phases plays a role. Understanding the interaction of actinides with these very variable substances, together with the complex chemical processes they are involved in, is a necessary prerequisite for predicting the chemistry and the migration behavior of acintides in natural and technical systems. This, in turn, forms the basis of safety analysis of radioactive waste repositories and contaminated sites. Therefore, a mechanistic understanding of the interaction of actinide and humics is crucial as a basis for the design of accurate, higher-level models of actinide chemistry and transport in the environment as well as for interpreting pertinent experiments and designing new ones.

Humic acids are considered to interact with actinide ions mainly via carboxylic groups, and experimental results, especially from EXAFS, suggest monodentate complexation of actinyls and other actinide ions by these groups. There are indications that phenolic OH groups also contribute to the complexation ability of humic substances. With reference

to these concepts, we mainly explored actinyl interactions with carboxylic and alcoholic groups with the help of relativistic density functional calculations, that also modeled solvent effects. Small carboxylic acids and alcohols were used as models of pertinent complexation sites of humic substances. We showed that already rather small organic molecules can be regarded as reasonable models, as the properties of the complexes did not change appreciably with the size of the model or their substituents. These results justified the omission of intended studies on larger models of humic substances. On the other hand, experience gained in this project strongly suggested a shift of focus on building more elaborate models of solvation, which turned out to be more involved than expected.

Our studies concentrated on the interaction of actinyls with a single organic molecule, mimicking an isolated complexation site of a humate molecule. We examined mainly uranyl(VI), but also neptunyl in the oxidation states (VI) and (V). Results on monocarboxylate complexes of uranyl with aliphatic and aromatic acids indicated somewhat stronger complexation interaction for aliphatic than for aromatic ligands. Monodentate structures turned out to be energetically preferred due to a strong hydrogen bond between an aqua ligand of the uranyl solvation shell and the carboxyl group (pseudo-bridging geometry), but the bidentate complexation mode turned out to be favored at the free energy level, due to stabilizing entropy effects. The latter findings are in line with crystal structures and common knowledge for carboxylate complexes, but are at variance with the prevailing interpretation of EXAFS results on actinyl humate complexes. The average length An-O_{eq} of actinyl oxygen bonds in the equatorial plane is regarded as important indicator. It is found at ~2.37 Å for the well studied case of uranyl; average distances of bidentate complexes are expected to be ~0.05 Å longer. At variance with this interpretation, our calculations yielded almost constant values for An-O_{eq} of about 2.37 Å, irrespective of the coordination mode and even of the chemical nature of the oxygen donor ligand (carboxylate, alcohol, alcoholate, hydroxide, water, ternary complexes). According to our model calculations, the only factor affecting the value of An-O_{eq} of solvated complexes is the coordination number of the complexes. Therefore, we suggested a re-interpretation of the EXAFS results as indicative for five-fold coordinated complexes. Unfortunately, the value of An-O_{eq} as the geometric parameter most commonly determined in experiment does not seem to be sensitive to the detailed structure and the chemical nature of an oxygen donor site. Therefore, a resolution of different An-O distances or measurement of other distances, e.g. An-C, is necessary for a further differentiation of the coordination modes. These findings also explain why blocking of phenolic OH groups of humic acids, which results in a change in the complexation behavior, is not reflected in the lengths of the actinyl bonds and the An-O_{eq} data determined experimentally. After all, carboxylic and alcoholic ligands were calculated to yield the same values for commonly used structural parameters.

As expected, our calculations showed that complexation of protonated alcoholic groups proceed with lower barriers when the alcoholic group is deprotonated in the field of the actinyl ion. This mechanism may allow actinide complexation by alcoholic groups even at moderate pH values, especially for multiply charged species.

Complexation energies of the species studied were determined mainly via exchange reactions involving aqua ligands. While experimentally accessible geometric parameters gave a rather uniform picture of bonding, ligand exchange energies vary stronger, hence are more sensitive. These results support empirical models of actinide humate complexation which assume a broad range of bond strengths of complexation sites. Summarizing the consequences of the results of this project on the interpretation of the atomistic structure and the energetics of actinyl humate complexation, we propose that these complexes, with a preferential coordination number of 5 for uranyl and neptunyl, should be regarded as bidentate, mainly involving carboxylic groups, but likely also other oxygen donor sites, e.g. hydroxyl groups.

In addition to the tasks laid out in the project proposal, we carried out accurate calculations of the heat of formation of uranyl(VI) and plutonyl(VI), fundamental quantities in actinide chemistry. Our results, 1527±42 kJ/mol for uranyl(VI) and 1749±63 kJ/mol for plutonyl(VI), improved earlier determinations and agree very well with recent experiments. As a side issue, not covered by this project, but inspired by the work of partners in the project consortium, we started to examine uranyl sorption at mineral surfaces using quantum mechanical methods. To the best of our knowledge, our study on uranyl sorption on alumina was the first accurate quantum mechanical modeling in this field [91]; the model results indicated outer sphere complexes to be preferred on the defect free (0001) surface of Al_2O_3.

As a support for the calculations in this project and also future work in actinide chemistry, the Douglas-Kroll-Hess approach to relativistic density functional chemistry was extended by an accurate and efficient method for a self-consistent relativistic treatment of the Coulomb interaction between electrons, which is modeled only at the nonrelativistic level in most other computational approaches. For an explicit and efficient modeling of extended solvation shells of solvated complexes, we developed a QM/MM/PCM procedure which currently employs a TIPnP force field for the water molecules. Test calculations on simplified model systems and the solvated uranyl ion demonstrated the quality and the efficiency of the approach, which should prove very useful in future projects.

This project brought unexpected insights into the atomic structure and energetics of actinyl complexes with organic functional groups. Our computational results turned out to be useful for interpreting currently available data on actinyl humate complexes. Thus we are confident that further work along these lines will be very worthwhile. Further studies are

expected to focus primarily on issues that were only briefly treated in this project. To complement the current project, a more thorough inspection of chelate complexation as well as complexation by more than a single functional group are suggested. Preliminary results of this project already showed that for carboxylic and alcoholic groups chelate structures do not necessarily result in complexes which are more stable than other complexation modes. Of particular interest will be studies of actinide ions in lower oxidation states, as the corresponding data base from experiments is incomplete. Results of the present project also suggest that further efforts directed at more detailed modeling of solvation will be beneficial for constructing more accurate models of actinide complexes in aqueous solution. Such method-oriented research is also a prerequisite for a more reliable determination of thermochemical parameters of these complexes – a major challenge to current quantum chemistry.

6 Publications Resulting from This Project

1) F. Schlosser; A Relativistic Density Functional Study of Actinide Complexation in Aqueous Solution, Dissertation, Technische Universität München, 2006.
2) L. V. Moskaleva, A. V. Matveev, J.Dengler, N. Rösch: The Heat of Formation of Gaseous PuO_2^{2+} from Relativistic Density Functional Calculations, Phys. Chem. Chem. Phys. 8, 3767-3773 (2006).
3) L. V. Moskaleva, V. A. Nasluzov, N. Rösch: Modeling Adsorption of the Uranyl Dication on the Hydroxylated α-Al_2O_3 (0001) Surface in an Aqueous Medium. Density Functional Study, Langmuir 22, 2141-2145 (2006).
4) F. Schlosser, S. Krüger, N. Rösch: A Density Functional Study of Uranyl Monocarboxylates, Inorg. Chem. 45, 1480-1490 (2006).
5) M. García-Hernández, C. Willnauer S. Krüger, L. V. Moskaleva, N. Rösch: Systematic DFT Study of Gas Phase and Solvated Uranyl and Neptunyl Complexes $[AnO_2X_4]^n$ (An = U, Np; X = F, Cl, OH, n = 2-; X = H_2O, n = 2+), Inorg. Chem. 45, 1356-1366 (2006).
6) L. V. Moskaleva, A. V. Matveev, S. Krüger, N. Rösch: The Heat of Formation of the Uranyl Dication: Theoretical Evaluation Based on Relativistic Density Functional Calculations, Chem. Eur. J. 12, 629-634 (2006).
7) S. Krüger, F. Schlosser, S. R. Ray, N. Rösch: Uranyl Complexation by Carboxylic Acids: A Relativistic Density Functional Model Study for Actinide Complexation by Humic Acids, Lecture Series on Computer and Computational Sciences 7, 904-907 (2006).
8) S. Krüger, F. Schlosser, N. Rösch: Monocarboxylate Complexes of Uranyl: A Relativistic Density Functional Study, in: Recent Advances in Actinide Science, R. Alvarez, N. D. Bryan, I. May (Eds.), Proceedings of the Conference Actinides 2005, Manchester, 2005, The Royal Society of Chemistry, Cambridge, 2006, p. 252-254.
9) V. Matveev, S. Majumder, N. Rösch: Efficient Treatment of the Hartree Interaction in the Relativistic Kohn-Sham Problem, J. Chem. Phys. 123, 164104, 1-8 (2005).

Further publications on results of this project and follow-up studies are in preparation.

References

[1] J. J. Katz, G. T. Seaborg, L.R. Morss (Eds.), The Chemistry of the Actinide Elements, 2. ed., Chapman and Hall, New York, 1986.

[2] L. R. Morss, N. M. Edelstein, J. Fuger (Eds.), Actinide and Transactinide Elements, 3. ed., Springer, Dordrecht, 2006.

[3] Z. Szabo, T. Toraishi, V. Vallet, I. Grenthe, Coord. Chem. Rev. 250 (2006) 784.

[4] Ref. 2, vol. 4, chap. 22.

[5] D. L. Clark, D. E. Hobart, M. P. Neu, Chem. Rev. 95 (1995) 25.

[6] K. H. Lieser, Radiochim. Acta 70/71 (1995) 355.

[7] R. J. Silva, H. Nitsche, Radiochim. Acta 70/71 (1995) 377.

[8] Ref. 2, vol. 4, chap. 23.

[9] F. J. Stevenson, Humus Chemistry, 2. Aufl., Wiley, New York, 1994.

[10] K. L. Nash, J. M. Cleveland, T. F. Rees, J. Environ. Radioact. 7 (1988) 131.

[11] G. R. Choppin, Radiochim. Acta 44/45 (1988) 23.

[12] M. A. Denecke, S. Pompe, T. Reich, H. Moll, M. Bubner, K. H. Heise, R. Nicolai, H. Nitsche, Radiochim. Acta, 79 (1997) 151.

[13] S. Sachs, K. Schmeide, T. Reich, V. Brendler, K. H. Heise, G. Bernhard, Radiochim. Acta, 93 (2005) 17.

[14] K. Schmeide, T. Reich, S. Sachs, V. Brendler, K. H. Heise, G. Bernhard, Radiochim. Acta, 93 (2005) 187.

[15] M. A. Denecke, T. Reich, S. Pompe, M. Bubner, K. H. Heise, H. Nitsche, P. G. Allen, J. J. Bucher, N. M. Edelstein, D. K. Shuh, J. Phys. IV 7, C2 (1997) 637.

[16] S. Pompe, K. Schmiede, M. Bubner, G. Geipel, K. H. Hiese, G. Bernhard, H. Nitsche, Radiochim. Acta 88 (2000) 553.

[17] K. Schmiede, S. Sachs, M. Bubner, T. Reich, K. H. Hiese, G. Bernhard, Inorg. Chim. Acta 351 (2003) 133.

[18] S. Sachs, G. Bernhard, Radiochim. Acta 93 (2005) 141.

[19] M. A. Denecke, Coord. Chem. Rev. 250 (2006) 730.

[20] P. Lubal, D. Fetsch, D Siroky, M. Lubalova, J. Senkyr, J. Havel, Talanta 51 (2000) 977.

[21] D. Schild, C. M. Marquardt, Radiochim. Acta 88 (2000) 587.

[22] K. Schmeide, T. Reich, S. Sachs, V. Brendler, K. H. Heise, G. Bernhard, Radiochim. Acta 93 (2005) 187.

[23] S. Pompe, A. Brachmann, M. Bubner, G. Geipel, K. H. Heise, G. Bernhard, H. Nitsche, Radiochim. Acta 82 (1998) 89.

[24] J. I. Kim in: Handbook of the Physics and Chemistry of the Actinides; A. J. Freeman, C. Keller (Eds.), Elsevier, Amsterdam, 1986, Chapter 8.

[25] A. Krepelova, S. Sachs, G. Bernhard, Radiochim. Acta 94 (2006) 825.

[26] V. Vallet, Z. Szabó, I. Grenthe, Dalton Trans. (2004) 3799.

[27] V. Vallet, P. Macak, U. Wahlgren, I. Grenthe, Theor. Chem. Acc. 115 (2006) 145.

[28] N. Kaltsoyannis, P. J. Hay, J. Li, J.-P. Blaudeau, B. E. Bursten, in Ref. 2, vol. 3, chap. 17.

[29] Moll, H.; Geipel, G.; Reich, T.; Bernhard, G.; Fanghänel, T.; Grenthe, I. Radiochim. Acta 91 (2003) 11.

[30] J. Jiang, L. Rao, P. Di Bernardo, P. L. Zanonato, A. Bismondo, J. Chem. Soc., Dalton Trans. 8(2002) 1832.

[31] P. G. Allen, J. J. Bucher, D. K. Shuh, N. M. Edelstein, T. Reich, Inorg. Chem., 36 (1997) 4676.

[32] N. Rösch, S. Krüger, M. Mayer, V. A. Nasluzov The Douglas-Kroll-Hess Approach to Relativistic Density Functional Theory: Methodological Aspects and Applications to Metal Complexes and Clusters, in: Recent Developments and Applications of Modern Density Functional Theory, J. M. Seminario (Eds.), Theoretical and Computational Chemistry Series, Bd. 4, Elsevier, Amsterdam, 1996, S. 497.

[33] N. Rösch, A. V. Matveev, V. A. Nasluzov, K. M. Neyman, L. Moskaleva, S. Krüger Quantum Chemistry with the Douglas-Kroll-Hess Approach to Relativistic Density Functional Theory: Efficient Methods for Molecules and Materials, in: Relativistic Electronic Structure Theory-Applications, P. Schwerdtfeger (Eds.) Theoretical and Computational Chemistry Series, Elsevier, Amsterdam, 2004, S. 656.

[34] T. Belling, T. Grauschopf, S. Krüger, F. Nörtemann, M. Staufer, M. Mayer, V. A. Nasluzov, U. Birkenheuer, A. Hu, A. V. Matveev, A. M. Shor, M. Fuchs-Rohr, K. Neyman, D. I. Ganyushin, T. Kerdcharoen, A. Woiterski, A. Gordienko, S. Majumder, N. Rösch, ParaGauss, Version 3.0, Technische Universität München, 2004.

[35] M. S. K. Fuchs, A. M. Shor, N. Rösch, Int. J. Quantum Chem. 86 (2002) 487.

[36] Y. Dudal, F. Gerard, Earth-Science Revs. 66 (2004) 199.

[37] L. K. Koopal, T. Saito, J. P. Pinheiro, W. H. Riemsdijk, Colloids Surf. A 265 (205) 40.

[38] B. A. Hess (Hrsg.), Relativistic Effects in Heavy Element Physics and Chemistry, Wiely, Chichester, 2003, Kap. 3.

[39] X. Cao, M. Dolg, Coord. Chem. Rev. 250 (2006) 900.

[40] L. Belkhiri, R. Lissillour, A. Boucekkine, J. Mol. Struct. Theochem 757 (2005) 155.

[41] G. A. Shamov, G. Schreckenbach, J. Phys. Chem. A 109 (2005) 10961.

[42] C. Clavaguéra-Sarrio, V. Vallet, D. Maynau, C. J. Marsden, J. Chem. Phys. 121 (2004) 5312.

[43] E. Fromager, V. Vallet, B. Schimmelpfennig, P. Macak, T. Privalov, U. Wahlgren, J. Phys. Chem. A 109 (2005) 4957.

[44] J. Tomasi, Theor. Chem. Acc. 112 (2004) 184.

[45] Z. Cao, K. Balasubramanian, J. Chem. Phys. 123 (2005) 114309.

[46] L. V. Moskaleva, S. Krüger, A. Spörl, N. Rösch, Inorg. Chem. 43 (2004) 4080.

[47] F. Schlosser, Dichtefunktionaluntersuchungen an zweikernigen Uranylkomplexen, Diplomarbeit, Technische Universität München, 2001

[48] K. E. Gutkowski, D. A. Dixon, J. Phys. Chem. A 110 (2006) 8840.

[49] V. Vallet, U. Wahlgren, B. Schimmelpfennig, H. Moll, Y. Szabó, I. Grenthe, Inorg. Chem. 40 (2001) 3516.

[50] B. Siboulet, C. J. Marsden, P. Vitorge, Chem. Phys. 326 (2006) 289.

[51] I. Infante, B. van Stralen, L. Vischer, J. Comp. Chem. 27 (2006) 1156.

[52] I. Infante, L. Vischer, J. Comp. Chem. 25 (2004) 386.

[53] M. Bühl, R. Diss, G. Wipff, J. Am. Chem. Soc. 127 (2005) 13506.

[54] M. Bühl, H. Kabrede, Inorg. Chem. 45 (2006) 3836.

[55] M. Bühl, H. Kabrede, Chem. Phys. Chem. 7 (2006) 2290.

[56] M. Bühl, H. Kabrede, R. Diss, G. Wipff, J. Am. Chem. Soc. 128 (2006) 6357.

[57] W. Chien, V. Anbalagan, M. Zandler, M. Van Stipdonk, D. Hanna, G. Gresham, G. Goenewold, J. Am. Soc. Mass. Spectrom. 15 (2004) 777.

[58] W. A. de Jong, E. Aprà, T. L. Windus, J. A. Nichols, R. J. Harrison, K. E. Gutowski, D. A. Dixon, J. Phys. Chem. A 109 (2005) 11568.

[59] F. Schlosser, S. Krüger, N. Rösch, Inorg. Chem. 45 (2006) 1480.

[60] F. Schlosser, Dissertation, Technische Universität München, 2006.

[61] J. Leciejewicz, N. W. Alcock, T. J. Kemp, Struct. Bonding 82 (1996) 43.

[62] D. H. Templeton, A. Zalkin, H. Ruben, L. L. Templeton, Acta Cryst. C41 (1985) 1439.

[63] J. Vázquez, C. Bo, J. M. Poblet, J. de Pablo, J. Bruno, Inorg Chem. 42 (2003) 6136.

[64] F. A. Cotton, G. Wilkinson, Advanced Inorganic Chemistry, 5th ed., Wiley, New York, 1988, p. 980-993.

[65] S. Krüger, F. Schlosser, N. Rösch in: Recent Advances in Actinide Science, R. Alvarez, N. D. Bryan, I. May (Eds.), Proceedings of the Conference Actinides 2005, Manchester, 2005, The Royal Society of Chemistry, Cambridge, 2006, p. 252.

[66] L. Rao, J. Jiang, P. Zanonato, P. Di Bernardo, A. Bistondo, a. Y. Garnov, Radiochim. Acta 90 (2002) 581.

[67] H. Nitsche, R. J. Silva, V. Brendler, T. Geipel, T. Reich, Y. A. Teterin, M. Thieme, L. Baraniak, G. Bernhard, G. in: Actinide Speciation in High Ionic Strength Media; Ed. D. T. Reed, S. B. Clark, L. Rao, Kluwer Academic/Plenum Publishers: New York, 1999, S. 11.

[68] S. Krüger, F. Schlosser, S. R. Ray, N. Rösch Lecture Series on Computer and Computational Sciences 7 (2006) 904.

[69] F. Quilès, A. Burneau, Vibr. Spectros., 18 (1998) 61.

[70] C. Nguyen-Trung, G. M. Begun, D. A. Palmer, Inorg. Chem. 31 (1992) 5280.

[71] M. A. Denecke, T. Reich, M. Bubner, S. Pompe, K. H. Heise, K. H. Nitsche, P. G. Allen, J. J. Bucher, N. M. Edelstein, D. K. Shuh, J. All. Comp., 271 (1998) 123.

[72] B. F. Mentzen, H. Sautereau, Acta Cryst, B36 (1980) 2051.

[73] S. R. Ray, S. Krüger, N. Rösch, in preparation.

[74] S. Pompe, K. Schmeide, M. Bubner, G. Geipel, K. H. Heise, G. Bernhard, H. Nitsche, Radiochim. Acta 88 (2000) 553.

[75] S. Sachs, G. Bernhard. Radiochim. Acta 93 (2005) 141.

[76] K. Schmeide, S. Sachs, M. Bubner, T. Reich, K. H. Heise, G. Bernhard. Inorg. Chim. Acta 351 (2003) 133.

[77] A. Kremleva, S. Krüger, N. Rösch, in preparation.

[78] C. J. Carrell, H. L. Carrell, J. Erlebacher, J. P. Glusker, J. Am. Chem. Soc. 110 (1988) 8651.

[79] L. V. Moskaleva, A. V. Matveev, S. Krüger, N. Rösch, Chem. Eur. J. 12 (2006) 629.

[80] L. V. Moskaleva, A. V. Matveev, J.Dengler, N. Rösch, Phys. Chem. Chem. Phys. 8 (2006) 3767.

[81] J. K. Gibson, R. G. Haire, M. Santos, J. Marçalo, A. P. de Matos, J. Phys. Chem. A 109 (2005) 2768.

[82] H. H. Cornehl, C. Heinemann, J. Marçalo, A. P. de Matos, H. Schwarz, Angew. Chemie 35 (1996) 650; Angew. Chemie Int. Ed. Engl. 35 (1996) 891.

[83] A. V. Matveev, N. Rösch, J. Chem. Phys. 118 (2003) 3997.

[84] A. V. Matveev, S. Majumder, N. Rösch, J. Chem. Phys. 123 (2005) 164104.

[85] M. Mayer, S. Krüger, N. Rösch, J. Chem. Phys. 115 (2001) 4411.

[86] A. V. Matveev, N. Rösch, J. Chem. Phys. 118 (2003) 3997.

[87] H. Lin, G. T. Truhlar, Theor. Chem. Acc. 117 (2007) 185

[88] T. Kerdcharoen, U. Birkenheuer, S. Krüger, A. Woiterski, N. Rösch, Theor. Chem. Acc. 109 (2003) 285.

[89] W. L. Jorgensen, J. Chandrasekhar, J. D. Madura, R. W. Impey, M. Klein, J. Chem. Phys. 79 (1983) 926.

[90] J. Zielkiewicz, J. Chem. Phys. 123 (2005) 104501.

[91] L. V. Moskaleva, V. A. Nasluzov, N. Rösch, Langmuir 22 (2006) 2141.